Research Square

Preprints are preliminary reports that have not undergone peer review.
They should not be considered conclusive, used to inform clinical practice,
or referenced by the media as validated information.

Spatial non-stationary relationship between temperature and precipitation variation patterns and drought in the southwestern Caspian Sea

Mahmoud Roshani

m.roshani1976@gmail.com

Kharazmi University

Leila Haghparast Mojdehi

Islamic Azad University

Bahman Ramezani Gourabi

Islamic Azad University

Atoosa Bigdeli

Islamic Azad University

Yousef Zeinolabedin Amuoghin

Islamic Azad University

Sedigheh Ganji Goufali

Islamic Azad University

Fatemeh Hakimi Shirayeh

Iowa State University

Research Article

Keywords: Drought, OLS regression, non-stationarity, Anselin Local Moran's I (ALMI), Caspian Sea

Posted Date: November 3rd, 2026

DOI: https://doi.org/10.21203/rs.3.rs-11586932/v1

License: This work is licensed under a Creative Commons Attribution 4.0 International License.
Read Full License

Additional Declarations: No competing interests reported.

Spatial non-stationary relationship between temperature and precipitation variation patterns and drought in the southwestern Caspian Sea

Mahmoud Roshani[1]

[1]PhD in Climatology, Department of Physical Geography, Kharazmi University, Tehran, Iran

Email: m.roshani1976@gmail.com https://orcid.org/0009-0001-4667-2991

Leila Haghparast Mojdehi[2]

[2]PhD in Climatology, Faculty of Humanities, Islamic Azad University, Rasht Branch, Guilan, Iran

Email: leilahaghparast@gmail.com https://orcid.org/0009-0000-3055-9305

Bahman Ramezani Gourabi[3]

[3]Department of Physical Geography, Faculty of Literature and Humanities, Islamic Azad University, Rasht, Iran

Email: Bahmanr2000@gmail.com https://orcid.org/0000-0002-1213-8547

Atoosa Bigdeli[4]

[4]Department of Physical Geography, Faculty of Literature and Humanities, Islamic Azad University, Rasht, Iran

Email: bigdeli_atoosa@yahoo.com https://orcid.org/0000-0002-8760-8689

Yousef Zeinolabedin Amuoghin[5]

Email: yousef.zeinolabedin@iau.ac.ir https://orcid.org/0000-0003-3661-0006

[4]Department of Human Geography, Faculty of Literature and Humanities, Islamic Azad University, Rasht, Iran

Sedigheh Ganji Goufali[6]

[6]PhD in Climatology, Faculty of Humanities, Islamic Azad University, Najafabad Branch, Isfahan, Iran

Email: sedigheh.ganji95@gmail.com https://orcid.org/0009-0004-1234-9012

Fatemeh Hakimi Shirayeh[7]

[7]PhD Student in Environmental Sciences, Department of Agronomy, Iowa State University, Ames, Iowa, USA

Email: fatemeh9@iastate.edu https://orcid.org/0009-0003-4430-5471

Abstract

One of the consequences of temperature and precipitation variation is drought, the continuation of which is accompanied by destructive environmental effects and depletes surface and groundwater resources. In this study, the most significant consequence of variation in temperature and precipitation—namely, drought—is examined and analyzed. To this end, the required data were first obtained from the European Centre for Medium-Range Weather Forecasts (ECMWF) at a spatial resolution of 0.25° × 0.25°

for a 44-year period (1980 to 2023). Subsequently, the trends in the SPI and RDI indices were determined using the Mann-Kendall trend test, and the Anselin Local Moran's I (ALMI) statistic was employed to identify the type of their spatial patterns. In addition, ordinary least squares (OLS) regression was used to determine the relationship and harmony of the variables across Guilan Province. The results showed that the RDI index exhibited a negative, decreasing trend in the months of March, May, June, and August. Furthermore, the results of this analysis regarding the mean SPI index indicate a negative trend during the months of May, June, and August; it should also be noted that the intensity of both the RDI and SPI indices increased during the period. Given that average precipitation during the months of May, June, and August follows a decreasing trend, a corresponding decreasing trend in the drought indices has also become significant. In addition to a negative trend in the mean RDI index for the months of March, May, June, and August, a negative trend in the RDI index for all cells during these months was also confirmed. Furthermore, the results obtained from the MK trend test for the SPI index of the cells in August confirm a negative trend, which is consistent with the findings from the same test applied to the mean SPI index for August. In this regard, spatial analysis of the RDI and SPI drought index trend test indicates that the high-high (HH) and low-low (LL) cluster patterns have formed as separate zones in different parts of the province, from the plains to the mountains and from east to west, in March, May, June, and August. Also, a very good spatial relationship was obtained between SPI and precipitation in all months of the year (except October). Furthermore, the spatial relationship between the variables RDI and precipitation, as well as between RDI and SPI, was significant at the 0.05 level during certain months. Overall, it can be stated that non-random behavior governs the spatial patterns of the RDI and SPI indices as well as precipitation, and there is a notable spatial correspondence among them.

Keywords: Drought, OLS regression, non-stationarity, Anselin Local Moran's I (ALMI), Caspian Sea

1. Introduction

Since the Industrial Revolution, the Earth's annual temperature has risen by more than 1°C. Between 1880 and 1980—the period for which data have been recorded—temperatures increased by an average of 0.07°C (0.13°F) every 10 years. However, since 1981, the rate of increase has more than doubled. In other words, over the past 40 years, we have witnessed an increase in global temperatures of 0.18°C per decade. The conclusion is that Earth has never been warmer than this. In other words, 9 of the 10 warmest years have occurred since 2005, and the 5 warmest years on record have all occurred since 2015. Climate scientists have now concluded that if we are to avoid a future where daily life across the globe is confronted by the worst and most destructive impacts of climate change—such as severe droughts, wildfires, floods, tropical storms, and other natural disasters—global warming must be limited to 1.5°C by 2040 (IPCC, 2023; Surampalli et al., 2013; Chirgwin, 2012).

In recent years, the unprecedented rate of global warming has had potentially profound effects on natural ecosystems and human societies. For example, an increase in natural hazards, the acceleration of the hydrological and carbon cycles, a decline in food security, and the facilitation of the geographical spread of many infectious diseases are among the consequences of climate change, which have imposed serious economic and health-related damage on societies (Dottori et al., 2018; Sun et al., 2019; Surendran Nair et al., 2020; Watts et al., 2020). Recent studies indicate that the likely range for the increase in global temperature is 2 to 4.9°C; consequently, warming levels of 1.5, 2, 3, and 4°C represent significant milestones—not only for mitigation efforts but also for understanding the anticipated impacts of climate change (Raftery et al., 2017).

Studies conducted across Iran and other parts of the world confirm significant changes in climatic variables—specifically temperature and precipitation. For example, an analysis of the trend of precipitation changes in northwestern Iran over the past half century indicates a decreasing trend, and months with a negative trend are more numerous than months with a positive trend (Mirabassi & Dinpazhooh, 2013). Temperature and precipitation variations along the southern coast of the Caspian Sea—when compared with variations on a global scale and across the Northern Hemisphere—indicate that a decrease in temperature is accompanied by a decrease in precipitation, while an increase in temperature is associated with an increase in precipitation. Furthermore, the minimum temperatures at the three stations of Ramsar, Babolsar, and Gorgan show a more pronounced increase compared to the maximum temperatures; this may be attributed to the rise in greenhouse gases, which has a greater impact on the increase in minimum temperatures (Pirnia et al., 2015). In this context, an assessment and understanding of climate change in

Iran over recent decades indicate that extreme heat indices—such as summer days, warm days, warm nights, and tropical nights—are on the rise; conversely, trends for extreme cold indices—including frost days, cold nights, and cold days—are negative, indicating a decline. Heat waves are becoming longer, while cold waves are becoming shorter; overall, the frequency of extreme precipitation events is on the rise (Darand, 2015). Furthermore, an analysis of the trends and spatial patterns of annual and seasonal precipitation in the western half of Iran reveals the presence of intra-decadal variations and patterns of positive spatial autocorrelation. In more recent periods—with the exception of winter, which has experienced a negligible increasing trend—the spatial extent of positive spatial autocorrelation in precipitation has diminished on an annual basis, as well as during the spring and autumn seasons (Ghiasabadi Farahani et al., 2018). Furthermore, studies conducted by Soleimani Sardoo & Mesbahzadeh (2021), Zarrin & Dadashi-Roudbari (2022, 2023), Mirshekaran et al. (2021), Derakhshi et al. (2024), and Doulabian et al. (2021) confirmed the existence of significant changes in temperature and precipitation, as well as irregularities in the spatiotemporal occurrence of these two variables, within Iran's future climate. Similarly, studies conducted by Zahid & Rasul (2010) in Pakistan, Alina & Irina (2013) in the Oltenia Plain, Nicholson et al. (2018) on the African continent, Gomez-Gomez et al. (2022) in the Mediterranean region, and Mathbout et al. (2023) in Syria suggest that significant changes in temperature and precipitation are likely in the future for these regions. Given that drought is directly influenced by changes in precipitation and temperature, this phenomenon poses an increasing threat to human society in the future.

Heterogeneity in the phenomenon of drought arises from the spatial variability of temperature and precipitation; consequently, this phenomenon exhibits strong spatial heterogeneity due to the factors that influence it. Owing to spatial inhomogeneity, predicting the spatial and temporal patterns of drought in different geographical regions remains a challenge (Shi et al., 2022). The study by Wang et al. (2025) on the Yellow River basin in Inner Mongolia indicated that the strongest interactive effects on the heterogeneity of the CWSI drought index occur between precipitation and temperature, and between precipitation and elevation. Consequently, drought within the basin is governed more by ET than by PET, and is driven by the interplay of meteorological factors (precipitation, temperature) and topographical factors (DEM). Nejadrekabi et al. (2021) using two spatial statistical indices—namely Local Moran's I (LMI) and hot spot analysis (Getis-Ord Gi*)—identified high-high clusters of precipitation in the northeast, as well as hot spot clusters for both the SPI and SPEI indices in the southern and southwestern regions of Khuzestan. Here, the spatial inconsistency between precipitation and drought is quite evident. Furthermore, a spatiotemporal

117 analysis of drought using the SPI and SPEI indices in China's Sichuan Province revealed that elevation (H) is not the
118 primary factor influencing the spatial heterogeneity of precipitation in the province; rather, precipitation levels are
119 jointly determined by elevation (H), temperature (T), longitude (Lo), and latitude (La) (Liu et al., 2021). The
120 spatiotemporal pattern of drought characteristics in the Yellow River Basin (YRB) reveals heterogeneity; specifically,
121 the phenomenon shows a significant increase in the northwestern and downstream regions, and a significant decrease
122 in the central part of the basin. Furthermore, precipitation and temperature were the most direct factors influencing
123 the severity of drought, and they exerted a significant impact on both the upper and lower limits of drought severity
124 (Gao et al., 2023). In their examination of the spatial heterogeneity of agricultural drought drivers, Shi et al. (2025)
125 argue that elevation accounts for the greatest spatial variability of drought in China's Hetao irrigation region.
126 Furthermore, the temperature factor consistently influences the severity of drought across the sub-regions. Meanwhile,
127 potential evapotranspiration (PET) and runoff have demonstrated their influence on the spatial heterogeneity of
128 agricultural drought across sub-regions. As previously mentioned, various factors influence drought and its severity;
129 a proper understanding of the impact of drought on a given region can only be achieved when all factors contributing
130 to its intensification, or conversely, its mitigation and weakening, are taken into account. In the aforementioned studies,
131 the primary emphasis was placed on the factors and drivers influencing the spatial heterogeneity of drought; however,
132 the spatial harmony and disharmony between the variables used to calculate drought indices and the indices themselves
133 have not been addressed.
134 In this study, given the sensitive climatic conditions of the southern Caspian Sea coastal region, the harmony or
135 disharmony of temperature and precipitation with drought in Guilan Province is examined. In fact, the spatial
136 correspondence or non-correspondence of the two variables (temperature and precipitation) with the two drought
137 indices (SPI and RDI) is considered. In recent years, severe droughts have been observed in Guilan Province; the
138 resulting water scarcity and prolonged dry spells have caused numerous problems across various sectors—including
139 surface and groundwater resources, agriculture, and forests—as well as socio-economic issues. Regarding the
140 consequences of climate change, its catastrophic nature depends on the magnitude and speed of the changes, as well
141 as the damage it can cause to the Earth, humans, and other living beings. Furthermore, the extent of their vulnerability
142 and their response also depend on their level of resistance, resilience, and adaptability. Temperature and precipitation
143 are among the atmospheric variables that respond to climate change. These two variables are directly related to most
144 atmospheric phenomena; in other words, events such as droughts, wet or dry spells, severe floods, intense frosts,

145 storms, and the like stem from abnormal conditions in these two variables. Therefore, it is essential to study the
146 changes in the spatial patterns of temperature and precipitation in relation to the variations in the SPI and RDI indices
147 in this region of Iran. Furthermore, their spatial analysis can assist managers and policymakers across various
148 executive sectors in gaining awareness of the spatial variations of drought.

149 **2. Data & Methods**

150 **2.1. Study Area**

151 Guilan Province is situated along the southwestern coast of the Caspian Sea—spanning latitudes 36° 34′ to 38° 27′ N
152 and longitudes 48° 34′ to 50° 36′ E—and covers an area of 14,043.15 km^2, accounting for approximately 0.85% of
153 Iran's total land area. In terms of topography, this region consists of three zones—plains, foothills, and mountainous
154 areas—covering 4,576.15, 2,178.78, and 7,288.23 km^2, respectively; these account for 32.59, 15.51, and 51.9% of the
155 province's total area. This region is bounded to the north by the Caspian Sea, and to the south and west by the Alborz
156 mountain range; the Alborz heights serve as the boundary separating this region from the Iranian mainland, which lies
157 to its south. Its highest and lowest points are 3,690 m and -26 m.a.s.l. To examine the spatial harmony and disharmony
158 in the variations of the SPI and RDI indices in Guilan Province, monthly data on temperature, precipitation, and
159 evapotranspiration during a 44-year period (1980–2023) were utilized. Evapotranspiration was calculated based on
160 the C. W. Thornthwaite method. The website of the European Centre for Medium-Range Weather Forecasts (ECMWF)
161 was used to obtain the required data (https://www.ecmwf.int/). The latest set of reanalysis data from this site is called
162 ERA5, which provides highly accurate atmospheric data from 1979 onward. The data from this source are gridded,
163 and in this study, the range from 34°36′ to 38°27′ north latitude and 34°48′ to 36°50′ east longitude was selected for
164 data download. The spatial resolution of each cell was 0.25° × 0.25°, forming a 9×10 matrix that covers 90 cells per
165 measurement. Fig 1 shows the cells aligned with the boundaries of Guilan Province. Given the shape of the study area,
166 only 48 cells were selected out of 90.

167

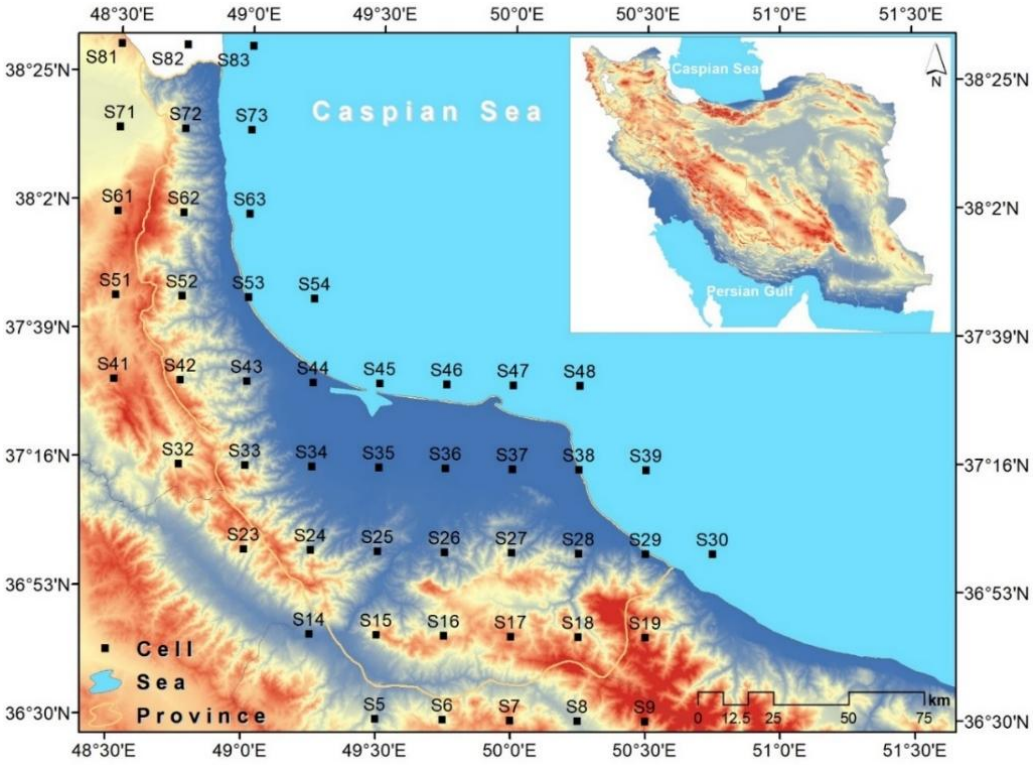


Fig 1. Grid covering the territory of Guilan Province (0.25° × 0.25°)

2.2. Methods

2.2.1. Mann-Kendall (MK) trend test

The Mann-Kendall trend test is a non-parametric test for identifying trends in time-series data. The initial value of the Mann-Kendall statistic (S) is assumed to be zero. If the next data value is greater than the previous one, it takes the value 1; otherwise, it takes the value -1. Suppose $x_1, x_2, \ldots . x_n$ is a set of n data points, where x_j represents the data point at time j. Then, the Mann-Kendall statistic is expressed as follows:

$$S = \sum_{k=1}^{n-1} \sum_{j=k+1}^{n} sign(x_j - x_k) \quad (1)$$

Here

$$sign(x_j - x_k) = \begin{cases} 1 & if \ x_j - x_k >= 0 \\ 0 & if \ x_j - x_k = 0 \\ -1 & if \ x_j - x_k < 0 \end{cases} \quad (2)$$

A very high positive value of S indicates an increasing trend, while a very low negative value indicates a decreasing trend. The variance S for a data series with n greater than 10 is equal to:

$$VAR(S) = \frac{1}{18}\left[n(n-1)(2n+5) - \sum_{p=1}^{g}(t_g - 1)(2t_p - 5)\right] \quad (3)$$

where n is the number of data points, g is the number of repeated groups, and tp is the number of data points in the p-th group. In the sequence 2, 3, 3, 3, where $n = 6$, $g = 2$, $t_1 = 2$, and $t_2 = 3$, the repeated value is 3. The normalized test statistic Z is calculated as follows:

$$\begin{aligned} Z &= \frac{S-1}{[VAR(S)]^{1/2}} \quad if \quad S > 0 \\ Z &= 0 \quad if \quad S = 0 \\ Z &= \frac{S+1}{[VAR(S)]^{1/2}} \quad if \quad S < 0 \end{aligned} \tag{4}$$

Additionally, the probability associated with the normalized test statistic must be calculated. The probability density function for a normal distribution with a mean of zero and a standard deviation of 1 can be calculated using the following equation.

$$f(z) = \frac{1}{\sqrt{2\pi}} e^{-\frac{z^2}{2}} \tag{5}$$

Here, the significance probability level is 95 percent. If Z is negative and the calculated probability is greater than the significance level, the trend is decreasing. If Z is positive and the calculated probability is greater than the significance level, the trend is increasing. If the calculated probability is less than the significance level, there is no trend in the data series (Gilbert, 1987).

2.2.2. Reconnaissance Drought Index (RDI)

To determine drought using RDI, monthly or annual total precipitation and potential evapotranspiration statistics should be used. Initially, for each year (i) within the statistical period under study, a value denoted as a_0 is calculated using the following formula:

$$a_0^{(i)} = \frac{\sum_{j=1}^{12} P_{ij}}{\sum_{j=1}^{12} ET_{ij}} \tag{6}$$

In this formula, P is precipitation and ET is potential evapotranspiration in the j-th month of year i. The value of i ranges from 1 to N. If precipitation and evapotranspiration are calculated on an annual basis, there will be no need to sum the monthly values in this formula. In the next step, an index is determined using the following equation, which is known as the normalized RDI index, or $RDI(n)$.

$$RDI_n^{(i)} = \frac{a_0^{(i)}}{\bar{a}_0} - 1 \tag{7}$$

In this equation, $\bar{a}_0$ is the arithmetic mean of the numbers a_0 of each year. Furthermore, the standardized index RDI (or $RDIs$) is calculated by first taking the logarithm of the values a_0, and subsequently computing their mean and standard deviation.

$$y_i = \ln a_0^{(i)} \quad (8)$$

We denote the mean and the standard deviation of these numbers by $\bar{y}_k$ and $\hat{\sigma}_{yk}$, respectively. Finally, the standardized RDI index is calculated using the following equation.

$$RDI_s^{(i)} = \frac{y_k^{(i)} - \bar{y}_k}{\bar{\sigma}_{yk}} \quad (9)$$

2.2.3. Standardized Precipitation Index (SPI)

To calculate the SPI index and convert precipitation values, the mean is first calculated.

$$\bar{x} = \frac{\sum_{i=1}^{n} x_i}{N} \quad (10)$$

It then becomes possible to interpret the standard score (Z), which has a mean of zero and a standard deviation of one.

$$S = \sqrt{\frac{\sum_{i=1}^{n}(x_i - \bar{x})}{N}} \quad (11)$$

The skewness can then be calculated using the following formula.

$$SK = \frac{N}{(N-1)(N-2)} \sum_{i=1}^{n} \left[\frac{x_i - \bar{x}}{S}\right]^2 \quad (12)$$

In the next step, the precipitation data are transformed to natural logarithms (Ln) and the average of these values is calculated. The transformed values are checked through the constant U, shape and scale:

$$\bar{x}_{Ln} = \frac{\sum_{i=1}^{n} Lnx_i}{N} \quad (13)$$

$$U = Ln(x_i) - \bar{x}_{Ln} \quad (14)$$

$$\beta = \frac{1}{4U}\left[1 + \sqrt{1 + \frac{4U}{3}}\right] \quad (15)$$

$$\alpha = \frac{\bar{x}}{\beta} \quad (16)$$

In this regard, the gamma function, which is a summarized exponential distribution, is used to interpret shape and scale values.

$$G(x) = \frac{1}{\alpha^{\beta}\Gamma\beta}\int_0^x x^{\beta-1} e^{-\frac{x}{\alpha}} dx \quad (17)$$

In this formula $\alpha, \beta > 0$and $x > 0$ and $\Gamma(\beta)$ is the gamma function. The gamma function is defined as follows.

$$\Gamma(\beta) = \int_0^{\infty} e^{-x} x^{\beta-1} dx \quad (18)$$

The mean and variance are calculated using the formulas $\mu = \alpha\beta$and $\delta^2 = \alpha^2\beta$, respectively (Marques desa, 2003). The two-parameter gamma function is not defined for zero values; therefore, its cumulative probability is:

$$F(x) = q + (1 - q)\, Gx \quad (19)$$

Here, $G(x)$ is the estimated distribution function—disregarding null values—and q represents the proportion of zeros in the cumulative precipitation series. SPI is a Z-score and indicates the deviation of the occurrence from the mean, expressed in standard deviation units. To calculate the Standardized Precipitation Index (SPI) by fitting a gamma probability density function to the frequency distribution, the precipitation data are first identified, and then the parameters α and β are calculated using the formulas provided above. Finally, by transforming the cumulative probability distribution of the gamma to the normal distribution, the SPI values are obtained. The simplest method for calculating SPI values is to use the Abramowitz–Stegun approximation, which is applied as follows. For $0 < H(x) \leq 0.5$ the value of t is equal to:

$$t = \sqrt{ln\left[\frac{1}{(H(x))^2}\right]} \quad (20)$$

And for $0.5 < H(x) \leq 1$, it will be given by the following formula:

$$t = \sqrt{ln\left[\frac{1}{(1 - H(x))^2}\right]} \quad (21)$$

Finally, the transformed gamma values are transformed a second time using the formulas below, based on the previously transformed values. In this case, if $0 < H(x) \leq 0.5$, the value of SPI can be calculated using the following formula.

$$SPI = -\left[t - \frac{c_0 + c_1 t + c_2 t^2}{1 + d_1 t + d_2 t^2 + d_3 t^3}\right] \quad (22)$$

And for $0.5 < H(x) \leq 1$, Formula 23 is used.

$$SPI = +\left[t - \frac{c_0 + c_1 t + c_2 t^2}{1 + d_1 t + d_2 t^2 + d_3 t^3}\right] \quad (23)$$

The constant values in equations 22 and 23, which are used in the SPI formula, are as follows.

$$c_0 = 2.515517 \quad c_1 = 0.802853 \quad c_2 = 0.010328$$

$$d_1 = 1.43278 \quad d_2 = 0.189269 \quad d_3 = 0.00130$$

Therefore, the Standardized Precipitation Index for a time transform t is derived using various formulas, based on the magnitude of the transformed gamma values. The obtained values are also used to determine 3, 6, 12, 18, 24, and 48-month droughts (Roshani et al., 2012).

2.2.4. Anselin Local Moran's I Statistic (ALMI)

For cluster and outlier analysis, the local Moran's I value, the Z-score, and the p-value—which indicates the significance of the index—are calculated. This statistic is derived based on the following equation.

$$I_i = \frac{x_i - \bar{x}}{S_i^2} \sum_{j=1, j\neq 1}^{n} w_{ij}\ w_{ij}(x_i - \bar{x}) \quad (24)$$

In this equation, x_i is the property of cell i, $\bar{x}$ is the mean of the corresponding property, and w_{ij} is the spatial weight between cells i and j. The value S_i^2 is obtained from the following .equation

$$S_i^2 = \frac{\sum_{j=1, j\neq 1}^{n} w_{ij}}{n-1} - \bar{x}^2 \quad (25)$$

In this equation, n is equal to the total number of features. In this statistic, the standard Z-score is calculated and tested at a specific confidence level. The standard score ZI_i is calculated as follows:

$$ZI_i = \frac{I_i - E[I_i]}{\sqrt{V[I_i]}} \quad (26)$$

In this case, the mathematical expectation $E[I_i]$ is equal to:

$$E[I_i] = -\frac{\sum_{j=1, j\neq 1}^{n} w_{ij}}{n-1} \quad (27)$$

And the variance $V[I_i]$ is equal to:

$$V[I_i] = E[I^2] - E[I_i]^2 \quad (28)$$

In this analysis, if the value of I_i is positive and significant, it indicates that the existing cells are surrounded by similar cells. Positive values of I_i indicate that a given cell—characterized by a specific value—is surrounded by cells with similar values (high-high or low-low); such cells are referred to as clusters. On the other hand, significant negative values of I_i indicate that the cell in question is surrounded by cells that are highly dissimilar in terms of their values (high-low or low-high); such cells are referred to as outliers, and their presence signifies negative spatial correlation (Roshani et al., 2021).

3. Results

3.1. MK Trend Test

The Mann-Kendall trend test was used to examine the significance of the trend in the mean temperature of Guilan Province. As shown in Table 1, the MK statistic for the months of January, February, March, April, May, and June was calculated to be 0.408, 0.391, 0.469, 0.171, 0.429, and 0.44, respectively. Considering the determined significance level, α=0.05, it is quite clear that the months in question, with the exception of April, have a significant trend, because the α_{cal} value is also less than 0.05. Furthermore, the values of the MK statistic for the months of July, August, September, October, November, and December were found to be 0.3, 0.423, 0.41, 0.33, 0.087, and 0.247, respectively. The α_{cal} value is lower than 0.05 in all cases (with the exception of November), and the significance of the trend is also confirmed. Consequently, the existence of a trend in the average temperatures of Guilan Province is confirmed

for 10 months of the year (all except April and November). Furthermore, a positive value for the MK statistic indicates a positive trend in the mean temperature of Guilan Province during the months under consideration. Therefore, over the past 44 years (1980 to 2023), the average temperature has steadily increased.

Table 1. Results of the MK trend test for the mean temperature of Guilan Province during different months of the year

Trend test	Jan	Feb	Mar	Apr	May	June	July	Aug	Sep	Oct	Nov	Dec
Kendall's statistics	0.408	0.391	0.469	0.171	0.429	0.44	0.3	0.423	0.41	0.33	0.087	0.247
S	386	370	444	162	406	416	284	400	388	312	82	234
Var(S)	9775	9775	9775	9775	9775	9775	9775	9775	9775	9775	9775	9775
P-value (2. tail)	***< 0.0001***	***0.000***	***< 0.0001***	0.103	***< 0.0001***	***< 0.0001***	***0.004***	***< 0.0001***	***< 0.0001***	***0.002***	0.413	***0.018***
α	0.05	0.05	0.05	0.05	0.05	0.05	0.05	0.05	0.05	0.05	0.05	0.05

The results of the MK trend test for average precipitation are presented in Table 2. The values of the Kendall statistic for the months of January through December were calculated as -0.034, -0.002, 0.053, 0.025, -0.205, -0.209, 0.127, -0.247, 0.011, -0.055, 0.066, and -0.055, respectively. No significant trend was observed for nine of these months; a significant negative trend in average precipitation was found only for the three months of May, June, and August. In other words, the average rainfall for the months of May, June, and August in this region has shown a significant decreasing trend between 1980 and 2023, resulting in a reduction in the average precipitation. Comparing the α_{cal} values with α = 0.05, it is evident that for the months of May, June, and August, this value is less than 0.05, confirming the significance of the trends. In the other months, the α_{cal} value is greater than 0.05, and the presence of a trend in their precipitation time series is rejected.

Table 2. Results of the MK trend test for average precipitation in Guilan Province during different months of the year

Trend test	Jan	Feb	Mar	Apr	May	June	July	Aug	Sep	Oct	Nov	Dec
Kendall's statistics	-0.034	-0.002	0.053	0.025	-0.205	-0.209	0.127	-0.247	0.011	-0.055	0.066	-0.055
S	-32	-2	50	24	-194	-198	120	-234	10	-52	62	-52
Var(S)	9775	9775	9775	9775	9775	9775	9775	9775	9775	9775	9775	9775
P-value (2. tail)	0.746	0.984	0.613	0.808	***0.049***	***0.045***	0.225	***0.018***	0.919	0.599	0.531	0.599
α	0.05	0.05	0.05	0.05	0.05	0.05	0.05	0.05	0.05	0.05	0.05	0.05

Tables 3 and 4 present the results of the MK trend test for the mean RDI and SPI in the study area. In this test, by comparing the α_{cal} at a 95% confidence level with an $\alpha = 0.05$, it is clearly evident that the α_{cal} values for the months of May, June, and August—for both indices—are less than $\alpha = 0.05$. Furthermore, the α_{cal} value for the RDI index in March is less than $\alpha = 0.05$, indicating a significant negative trend in the RDI and SPI index values during the months under consideration, while the trends for the remaining months are not statistically significant.

Table 3. Results of the MK trend test for mean RDI and SPI in Guilan Province during the first six months of the year

Trend test	Jan		Feb		Mar		Apr		May		June	
	RDI	SPI	RDI	SPI	RDI	SPI	RDI	SPI	RDI	SPI	RDI	SPI
Kendall's statistics	-0.175	-0.011	-0.116	0.011	-0.245	0.099	0.044	0.032	-0.214	-0.214	-0.233	-0.209
S	-166	-10	-110	10	-232	94	42	30	-202	-202	-220	-198

Var(S)	9775	9775	9775	9775	9775	9775	9775	9775	9775	9775	9775	9775
P-value (2. tail)	0.095	0.927	0.27	0.927	***0.019***	0.347	0.678	0.769	***0.042***	***0.042***	***0.027***	***0.046***
α	0.05	0.05	0.05	0.05	0.05	0.05	0.05	0.05	0.05	0.05	0.05	0.05

Table 4. Results of the MK trend test for mean RDI and SPI in Guilan Province during the second half of the year

Trend test	July		Aug		Sep		Oct		Nov		Dec	
	RDI	SPI	RDI	SPI	RDI	SPI	RDI	SPI	RDI	SPI	RDI	SPI
Kendall's statistics	0.11	0.133	-0.26	-0.249	0.004	0.059	-0.108	-0.03	0.112	0.099	-0.089	-0.004
S	104	126	-246	-236	4	56	-102	-28	106	94	-84	-4
Var(S)	9775	9775	9775	9775	9775	9775	9775	9775	9775	9775	9775	9775
P-value (2. tail)	0.298	0.206	***0.013***	***0.017***	0.976	0.578	0.307	0.785	0.288	0.347	0.401	0.976
α	0.05	0.05	0.05	0.05	0.05	0.05	0.05	0.05	0.05	0.05	0.05	0.05

3.2. Correlation Coefficient of Variables

Standardized precipitation (mm), temperature (°C), and the RDI and SPI indices are shown in Fig 2. This figure shows the variations in the above variables in terms of their temporal harmony or disharmony over a 44-year period, broken down by month of the year. The relationship between temperature and time indicates an increase in temperature for all months throughout the entire period. As shown in Table 5, there is a direct relationship between the temperature and time variables in all months except April and November, and this relationship is significant at two levels $\alpha = 0.05$ and $\alpha = 0.01$. The strength of the relationship varies between 0.416 and 0.677 and is considered relatively strong. The relationship of other variables with time, namely precipitation and the two indices SPI and RDI, is not significant in any month except for March, June, and August for SPI and August for RDI, as well as June and August for precipitation. Consequently, the increasing trend in temperature during March, May, June, and August shows an inverse relationship with the negative trends in precipitation (for June and August), the SPI (for May, June, and August), and the RDI (for March, May, June, and August); as temperatures rose throughout the period, the severity of drought during these months intensified (Fig 2). The existence of a trend and an inverse relationship between temperature and drought indices has been investigated in other studies such as Bazrafshan et al. (2017), Ghaemi et al. (2022), and Mohammadi et al. (2015), all of which report an increasing trend in drought severity in the historical and future periods. Furthermore, Ogunrinde et al. (2022) showed that temperatures will rise—both during the historical period and under future climate scenarios—leading to an increase in the intensity and frequency of the SPI, SPEI, and RDI indices. Also, Sayat et al. (2025) showed in the Southern Pre-Balkash region of Kazakhstan that increases in the intensity and frequency of drought periods are associated with climate change. Because climate change has caused an increase of 0.17 to 0.39°C per decade, and given the sensitivity of the SPEI index, the severity of droughts will increase.



Fig 2. Variations in precipitation (mm), temperature (°C), RDI, and SPI indices on the southwestern coast of the Caspian Sea during the period 1980–2023.

Table 5. Correlation coefficient (R), coefficient of determination (R^2), and significance level for the variables of precipitation, temperature, and the SPI and RDI indices.

Variable	Index	Jan	Feb	Mar	Apr	May	June	July	Aug	Sep	Oct	Nov	Dec
Precipitation (mm)	R^2	0.005	0.0006	0.025	0.009	0.056	0.089	0.058	0.092	0.007	0.015	0.0002	0.0038
	R	-0.069	0.025	0.159	0.095	-0.236	**-0.298***	0.24	***-0.304****	0.083	-0.121	-0.014	-0.062
	Sig. (2-tailed)	0.655	0.873	0.302	0.539	0.123	0.049	0.117	0.045	0.592	0.435	0.93	0.687
Temperature °C	R^2	0.277	0.373	0.458	0.076	0.329	0.399	0.185	0.217	0.368	0.225	0.036	0.175
	R	**0.526****	**0.611****	**0.677****	0.275	**0.574****	**0.632****	**0.430****	**0.466****	**0.607****	**0.474****	0.191	**0.419****
	Sig. (2-tailed)	0	0	0	0.07	0	0	0.004	0.001	0	0.001	0.215	0.005
SPI	R^2	0.05	0.029	0.128	0.0036	0.071	0.091	0.025	0.159	0.0004	0.032	0.001	0.026
	R	-0.224	-0.172	***-0.358****	0.06	-0.266	***-0.302****	0.157	***-0.399****	0.021	-0.18	0.032	-0.162
	Sig. (2-tailed)	0.143	0.264	0.017	0.697	0.081	0.046	0.309	0.007	0.893	0.242	0.836	0.294
RDI	R^2	0.0005	0.007	0.017	0.0055	0.048	0.069	0.038	0.142	0.008	0.012	0.0003	0.0038
	R	-0.023	0.083	0.131	0.074	-0.219	-0.264	0.196	***-0.377****	0.092	-0.11	0.017	-0.062
	Sig. (2-tailed)	0.882	0.592	0.397	0.632	0.152	0.083	0.203	0.012	0.552	0.479	0.911	0.691

Monthly variations in the SPI and RDI values for the study area throughout the period indicate a high degree of harmony between these two drought indices. However, when the intensity of drought or wetness increases, RDI values express drier or wetter climatic conditions than SPI values. Furthermore, there is good harmony between these two indicators at lower intensities, and most of the time the graphs coincide (Fig 3a). In this regard, the coefficient of determination (R^2) and the correlation coefficient (R) of these two indices were found to be 0.8449 and 0.9192, respectively, which indicates a strong relationship between the two indices SPI and RDI. Furthermore, 85% of the variations in the SPI index are explained by variations in the RDI index, and vice versa. Consequently, the strength of the relationship indicates a high degree of correspondence between these two variables (Fig 3b).

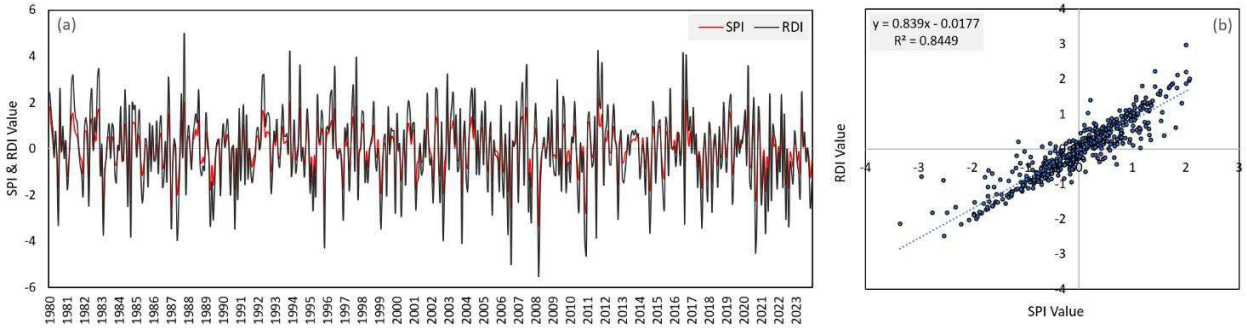


Fig 3. Monthly variations in SPI and RDI values for the study area during the 1980–2023 period (A). Relationship between RDI and SPI values during this period (B).

In addition to temporal changes in temperature and precipitation variables and SPI and RDI indices, spatial changes and their harmony or disharmony in space can be useful in drought prediction. For this purpose, first, ordinary least squares (OLS) regression of the Mann-Kendall trend statistic of the temperature, precipitation, SPI, and RDI variables was calculated to determine the degree of their spatial relationship, and then the harmony or disharmony of the patterns was assessed using the Anselin Local Moran's I (ALMI) method.

3.3. Spatial harmony and disharmony

3.3.1. Winter Months

Ordinary Least Squares (OLS) regression was used to determine the degree of spatial harmony or disharmony between the variables. The OLS method seeks to minimize the sum of squared errors (SSE) between the observed values and the predicted values:

$$SSE = \sum_{i=1}^{n} (y_i - \hat{y}_i)^2 \quad (29)$$

where y_i is the observed value for the ith data point. $\hat{y}_i$ is the predicted value for the ith data point, and n is the number of data points. The predicted values are obtained from the following linear model:

$$\hat{y}_i = \beta_0 + \beta_1 x_{i1} + \beta_2 x_{i2} + \ldots + \beta_p x_{ip} + \varepsilon \quad (30)$$

Here, β_0 is the intercept; $\beta_1, \beta_2, \ldots, \beta_p$ are the coefficients for the p properties; $x_{i1}, x_{i2}, \ldots, x_{ip}$ are the property values for the ith data point; and ε represents the random error term (residuals). Assuming these conditions are met, the OLS parameter estimator is determined as follows:

$$\beta = (x^T x)^{-1} x^T y \quad (31)$$

Here, β is the parameter vector of the general model to be estimated, and x is a matrix of predictors whose first-column elements are equal to 1. y represents the vector of observed values for the dependent variable, and $(x^T x)^{-1}$ is the inverse of the variance-covariance matrix (Nkeki & Osirike, 2013).

Tables 6 through 9 present the OLS regression values for the Mann-Kendall statistic regarding temperature, precipitation, the RDI index, and the SPI. As can be seen, OLS has been calculated for the relationships between temperature and RDI, precipitation and RDI, precipitation and SPI, and RDI and SPI, broken down by the months of the year. In January, the adjusted R^2 of the OLS model between RDI and temperature was 0.3349 and that between SPI and precipitation was 0.9999. The adjusted R^2 of the regression model between SPI and precipitation was very high, indicating that in January these two variables have a close relationship and the SPI value can be estimated from precipitation. Furthermore, the AIC values, as well as the joint F-statistic, the joint Wald statistic, and the Koenker (BP) statistic, are significant at the 95% confidence level (α=0.05). In this regard, there is again a significant relationship between SPI and precipitation in February and March (adjusted R^2 = 0.9998 and 0.999, respectively), because the OLS model evaluation statistics, namely F, Wald, and Koenker, are significant. Therefore, there is spatial harmony between the SPI variable and precipitation in each of the three months of the winter season, and their spatial variations are similar. Given that the p-value of the Koenker statistic is less than 0.05, the assumption of heteroscedasticity or non-stationarity within the geographical space under study can be considered significant for SPI

and precipitation. It should be noted that in January, the adjusted R^2 of the OLS model for RDI and temperature was 0.3349, which indicates that 33.49 percent of the changes in the dependent variable (RDI) can be explained by the explanatory variable (temperature), and the remaining percentage is related to variables that were not included in the model. The percentage of the dependent variable explained by the relationship between the SPI and precipitation during the three winter months is 99.99%—virtually 100%. Therefore, precipitation, as the explanatory variable, can be a very good estimator of the SPI drought index (the dependent variable). The Jarque-Bera statistic in Table 6 indicates whether the residuals (observed values of the dependent variable minus the predicted values) are normally distributed. The null hypothesis for this test is that the residuals are normally distributed. Given the statistical significance at a 95% confidence level (α=0.05), it can be concluded that there is a tendency toward spatial clustering in the residuals of the dependent variable.

Table 6. Ordinary Least Squares (OLS) regression of Moran's I statistic values for temperature, precipitation, RDI, and SPI during the winter months

Variables and Statistics	Winter Season											
	January				February				March			
Dependent Variable	RDI	RDI	SPI	RDI	RDI	RDI	SPI	RDI	RDI	RDI	SPI	RDI
Explanatory Variable	T	P	P	SPI	T	P	P	SPI	T	P	P	SPI
Intercept	0.1598	-0.1688	0.000013	-0.1687	0.0975	-0.1297	-0.0000	-0.1297	0.0260	-0.1931	-0.000087	-0.1932
Coefficient	-0.8511	0.1005	0.9992	0.1036	-0.6228	-0.3996	1.0005	-0.4007	-0.5413	-0.2548	1.000797	-0.2543
AICc	-33574	-27794	-183525	-27797	-30967	-30703	-16078	-30719	-36852	-37115	-138352	-37110
Multiple R^2	**0.3349**	0.0027	**0.9999**	0.0029	0.1634	0.1477	**0.9998**	0.1487	0.1182	0.1342	**0.999**	0.1339
Adjusted R^2	**0.3349**	0.0027	**0.9999**	0.0028	0.1633	0.1476	**0.9998**	0.1486	0.1181	0.1342	**0.999**	0.1339
Joint F-Statistic	7184	39.276	213528825	41.68	2786	2472	141213366	2492	1911	2212	41196283	2206
Joint Wald Statistic	4440.88	23.34	97532697	24.70	3374.3	2292.9	229317575	2309	2326	2672	38303434	2649
Koenker (BP) Statistic	598.899	2307.4	334.8469	2308.7	291.4	230.12	82.986	230.5	1299	599.3	134.01	594
Jarque-Bera Statistic	4268.20	4685.5	1019838.9	4643.8	1137.8	202.74	3364063	201.52	516	423.85	4552224	424

Therefore, the Anselin Local Moran's I (ALMI) was used to identify clusters and determine whether they exhibit spatial harmony or disharmony. Figure 4 displays the Anselin Local Moran's I (ALMI) statistics for temperature, precipitation, and the RDI and SPI drought indices during the winter months. The spatial pattern of temperature consists of two types of clusters: high-high (HH) and low-low (LL). In other words, in an HH cluster, high values of the Mann-Kendall trend test are surrounded by neighboring values that are also high, while in an LL cluster, low values of the Mann-Kendall trend test are surrounded by neighboring values that are also low. Based on Figure 4, it is clear that the ALMI pattern of temperature in January, February, and March in the southwest of Guilan province has HH values, and the northwest of this area from the plain to the mountains and the narrow strip of the central coast and part of its east (January) have LL values. Other regions exhibit random behavior in response to temperature changes. The ALMI pattern for the precipitation variable during the three winter months indicates a disharmony between the HH values of the temperature and precipitation variables. However, the harmony between the LL values of these two

variables increases in the northwest of the province. In other words, due to non-stationarity and spatial clustering, the areas of minimum temperature variation are somewhat consistent with the areas of minimum precipitation variation. In this regard, there is a clear spatial inconsistency between RDI values and temperature and precipitation values. However, the spatial pattern of SPI and precipitation is completely consistent, and the consistency of the two is confirmed by the adjusted R2 value for each of the three winter months.

3.3.2. Spring Months

Table 7 presents the calculations for the OLS regression for the months of the spring season. Based on the OLS results, there is a significant relationship between the RDI and precipitation, SPI and precipitation, and RDI and SPI in April at the α=0.05 level. Furthermore, the adjusted R^2 values for the aforementioned relationships are 0.7259, 0.9999, and 0.7271, respectively. This means that 72.59, 99.99, and 72.71 percent of the changes in the dependent variables (RDI, SPI, and RDI, respectively) can be explained by the explanatory variables. In other words, the independent variables of precipitation and SPI can be good estimators for the dependent variables of RDI, SPI, and RDI. In May, the relationship between the variables RDI and precipitation, SPI and precipitation, as well as RDI and SPI, is significant at the 0.05 level. The coefficient of determination of the dependent variable by the explanatory variable is 84.45, 99.99, and 84.36 percent, respectively, indicating that the explanatory variable can provide a good estimate of the values of the dependent variable in the studied space. In June, as in the other spring months, there is a very good relationship between the variables RDI and precipitation, SPI and precipitation, and RDI and SPI, with the coefficients of determination for this month being 92.62, 99.97, and 92.66 percent, respectively. Therefore, the precision of the estimator variable in June is higher than in April and May. Based on the significance of the AIC values, as well as the joint F-statistic, joint Wald statistic, and Koenker (BP) statistic, spatial consistency exists among the aforementioned variables and is statistically significant at the 0.05 level. The Jarque-Bera statistic indicates that the residuals—derived by subtracting the predicted values from the observed values of the dependent variable—are not normally distributed. Given that the Jarque-Bera statistic is statistically significant at the 0.05 level, this suggests the presence of non-stationarity and spatial clustering within the variables under investigation. Following the confirmation of spatial clusters in the residuals, Anselin Local Moran's I (ALMI) statistic was employed to examine the distribution of these clusters across the geographical space of the study area.

Table 7. Ordinary Least Squares (OLS) regression of Moran's I statistic values for temperature, precipitation, RDI, and SPI during the spring months

Variables and Statistics	Spring Season											
	April				May				June			
Dependent Variable	RDI	RDI	SPI	RDI	RDI	RDI	SPI	RDI	RDI	RDI	SPI	RDI
Explanatory Variable	T	P	P	SPI	T	P	P	SPI	T	P	P	SPI
Intercept	0.111081	0.0209	0.000057	0.020797	-0.20469	-0.07398	-0.000226	-0.073878	-0.26802	-0.022804	-0.000369	-0.02243
Coefficient	-0.304684	0.6967	0.999050	0.697947	0.10422	0.682827	0.998359	0.683548	0.14913	0.995279	0.998314	0.996992
AICc	-53669	-70182	-193449	-70243	-51516	-77964	-201524	-77874	-52819	-89876.62	-169645	-89941
Multiple R^2	0.128	**0.7259**	**0.9999**	**0.7271**	0.007725	**0.8445**	**0.9999**	**0.8436**	0.00939	**0.9262**	**0.9997**	**0.9266**
Adjusted R^2	0.127	**0.7259**	**0.9999**	**0.7271**	0.007655	**0.84455**	**0.9999**	**0.8436**	0.00932	**0.9262**	**0.9997**	**0.9266**
Joint F-Statistic	2095	37787	439252659	38009.9	111.05	77508.93	956178025	76934	135.22	179122.5	48304118	180002
Joint Wald Statistic	1020.4	39265	209437659	39760.4	107.542	107538.93	1043534547	106362	107.78	144564.3	30790691	146606
Koenker (BP) Statistic	2216	1415	110.17	1393.79	194.992	508.015	231.035	505.97	23.442	97.669	193.115	80.627
Jarque-Bera Statistic	111	1201	895.19	1211.27	1217.73	1418.27	225.429	1426.13	10975.14	38.467	4162636	56.3037

According to the cluster pattern created for the temperature variable in April, May, and June, the LL cluster of the temperature variable in the three spring months has some spatial similarity. This also holds true, to some extent, for the HH pattern of this variable during the spring months. The high-high (HH) values of the precipitation variable, located in the northwest of Guilan Province, exhibit spatial harmony during the three months of the spring season. The HH cluster of the RDI index overlapped somewhat in April, May, and June, and this was also true for the SPI (Fig 5). Overall, a significant difference is observed between the harmony of the temperature pattern during the spring months and the pattern of precipitation variability, as well as the RDI and SPI drought indices. This is clearly evident from the adjusted R^2 values in Table 7. HH and LL cluster patterns are observed in the precipitation, RDI, and SPI variables for the months of April, May, and June; notably, the HH cluster for precipitation in April shows strong harmony with the corresponding cluster in the RDI index. Also, the high-high (HH) cluster of the precipitation variable is completely consistent with the SPI index. The same is true for the LL cluster of the precipitation variable, the RDI index, and the SPI for April. The geographical distribution of the HH cluster is largely confined to the northwestern regions, while the LL cluster is restricted to the mountainous areas to the south of this region. Precipitation amounts, as well as the RDI and SPI indices, exhibit random behavior in other areas of the province. Spatial harmony between the HH and LL clusters of precipitation values, the RDI index, and the SPI was also evident in May; furthermore, the harmony observed in June is stronger than in the preceding two months, as the R^2 value for this month is higher than those for April and May (Fig 5).

3.3.3. Summer Months

The calculations related to the OLS regression for the summer months are presented in Table 8. As can be observed, there is consistency among the values of the Mann-Kendall trend statistic for the variables in the month of July during the summer season. The adjusted R^2 values for RDI and precipitation, SPI and precipitation, and RDI and SPI are 0.8504, 0.9996, and 0.8492, respectively; this indicates that the explanatory variable accounts for 85.04%, 99.96%,

and 84.92% of the variation in the dependent variable. The above values in the OLS regression equation indicate a good estimation of the dependent variable by the explanatory variable. This also applies to the months of August and September. Therefore, given precipitation, it is possible to easily estimate the two indices RDI and SPI. As previously mentioned, the joint F-statistic, the joint Wald statistic, and the Koenker (BP) statistic are significant at a 95% confidence level ($\alpha = 0.05$); this indicates that the regression model is appropriate and that there is spatial consistency between the explanatory and dependent variables. It should be noted that the null hypothesis in the joint F and joint Wald statistics is that the explanatory variable is not effective in the regression model. However, the statistical significance of the above statistics confirms the suitability of the model and the influence of the explanatory variable on the dependent variable. In this context, the significance of the Koenker (BP) statistic serves to determine whether the explanatory variables in the model—across both geographic space and data space—maintain a consistent relationship with the dependent variable. The results indicate that this statistic is significant at the $\alpha=0.05$ level, and the assumption that the relationship remains constant across both geographic space and data space is confirmed.

Next, the ALMI statistic for clusters, including HH and LL values, is examined to analyze spatial harmony between variables. The spatial harmony of the temperature variable in the three months of July, August, and September indicates good spatial similarity of HH and LL values in the study area. A spatial cluster of HH temperature values is observed in the central region, while an LL cluster is seen in the south and northwest of the province. The adjusted R^2 values for the temperature variable across different months of the summer season indicate the absence of a spatial relationship between this variable and precipitation, the RDI index, and the SPI. The lack of a relationship has also resulted in a lack of spatial harmony between them (Fig 6).

However, the ALMI statistic for the precipitation variable, as well as the RDI and SPI indices, indicates a significant relationship and spatial harmony among them. For example, in July, the west and east of the region follow the HH cluster pattern and its northwest follows the LL cluster pattern. In August, the spatial pattern changed compared to July: the HH pattern formed in the east of the region, and the LL pattern formed in its south and west. Furthermore, the spatial pattern of precipitation, as well as the RDI and SPI indices, exhibits an LL cluster pattern in the eastern part of the region, and an HH pattern in the southwestern part—extending, to some extent, into the western part.

Table 8. Ordinary Least Squares (OLS) regression of Moran's I statistics for temperature, precipitation, RDI, and SPI during the summer months

Variables and Statistics	Summer Season											
	July				August				September			
Dependent Variable	RDI	RDI	SPI	RDI	RDI	RDI	SPI	RDI	RDI	RDI	SPI	RDI

Explanatory Variable	T	P	P	SPI	T	P	P	SPI	T	P	P	SPI
Intercept	0.07331	-0.01317	-0.000103	-0.012985	-0.24602	-0.074216	0.000803	-0.074757	-0.018355	-0.04474	0.000076	-0.044789
Coefficient	0.10340	0.88062	1.000052	0.879835	-0.0291	0.787903	1.003599	0.785464	0.009027	0.78272	0.999464	0.782742
AICc	-54690	-81549	166879	-81442	-65428	-97847.83	-181413	-97996	-50291	-76688	-168222	-76626
Multiple R^2	0.0168	**0.8504**	**0.9996**	**0.8492**	0.001517	**0.8971**	**0.9998**	**0.8981**	0.000092	**0.8428**	**0.9998**	**0.8421**
Adjusted R^2	0.0168	**0.8504**	**0.9996**	**0.8492**	0.001447	**0.8971**	**0.9998**	**0.8981**	0.000022	**0.8428**	**0.9998**	**0.8421**
Joint F-Statistic	244.60	81074	41383726	80358	21.678	124347.92	70566364	125798	1.3168	76486.9	76253427	76090.99
Joint Wald Statistic	387.43	102828	58427288	102229	14.755	123694	52960629	126677	2.0329	43266	96910376	43117
Koenker (BP) Statistic	595.76	281.87	32.70	249.25	1679.72	55.578	187.688	56.30	152.221	485.16	85.39	469.81
Jarque-Bera Statistic	416.94	89.12	2227253	83.399	41.28	658.25	874506.82	690.71	3001.87	50.407	3467124	43.686

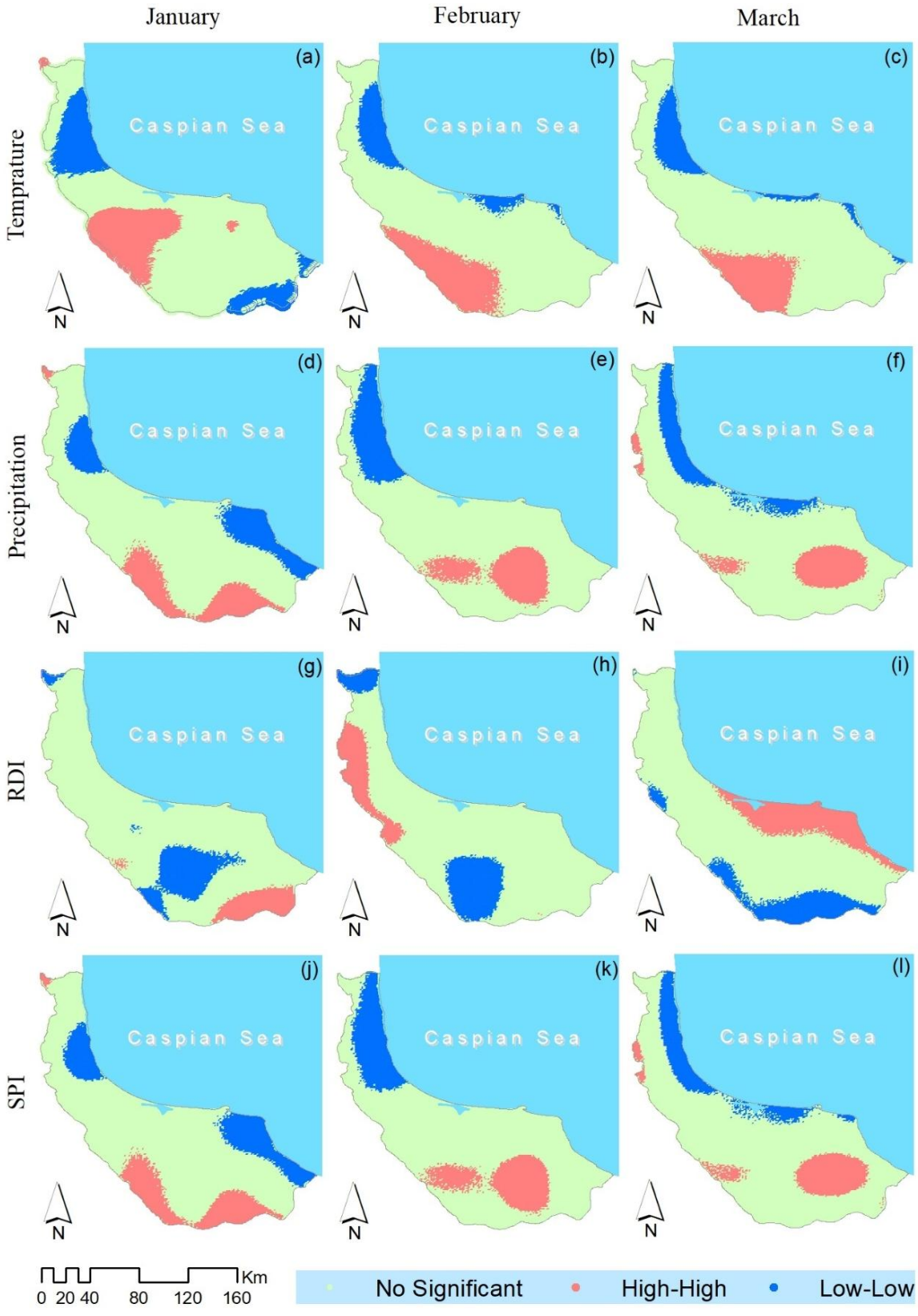


Fig 4. Anselin Local Moran's I (ALMI) statistics for temperature, precipitation, and the RDI and SPI drought indices, used to identify clusters and outliers, as well as their spatial harmony and disharmony during the winter months.

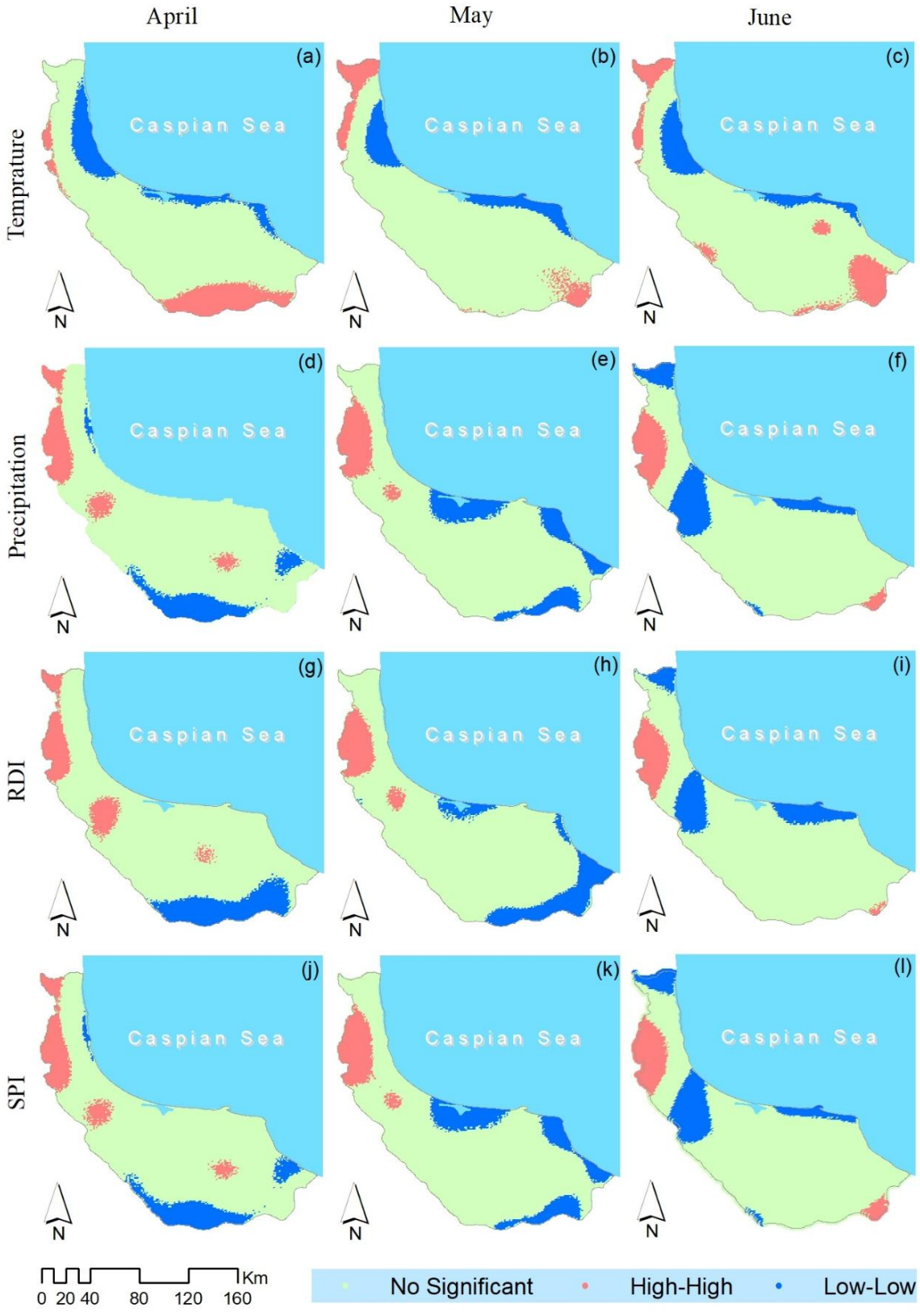


Fig 5. Anselin Local Moran's I (ALMI) statistics for temperature, precipitation, and the RDI and SPI drought indices, used to identify clusters and outliers, as well as their spatial harmony and disharmony during the spring months.

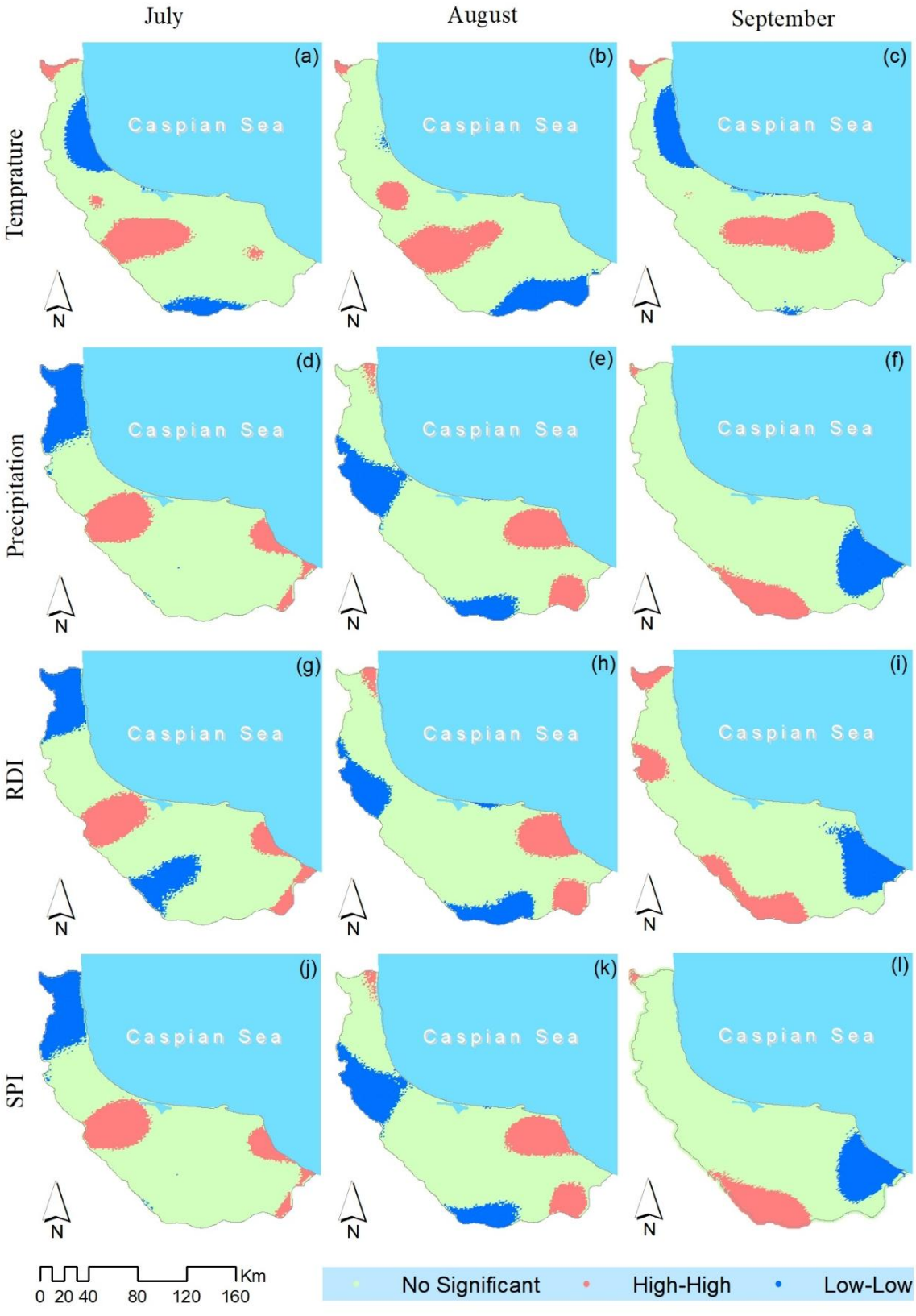


Fig 6. Anselin Local Moran's I (ALMI) statistics for temperature, precipitation, and the RDI and SPI drought indices, used to identify clusters and outliers, as well as their spatial harmony and disharmony during the summer months.

Other areas of Guilan Province exhibit random behavior with respect to the variables under study and are not significant at the 95% confidence level. Given the regularity obtained from the close relationship between the precipitation variable and the RDI and SPI indices in the summer months, any one of them can be used to predict the others. In addition, the non-stationarity of the variables in the study area has led to the emergence of clusters with different characteristics, with clear similarities between the clusters in the variables (with the exception of temperature).

3.3.4. Autumn Months

The results of the OLS regression analysis for the variables of temperature, precipitation, and the RDI and SPI indices for the autumn months are presented in Table 9. Based on the adjusted R^2 value (0.6875), there is a significant relationship between RDI and precipitation in October at the 95% confidence level. In this regard, there is no significant relationship between SPI and precipitation, and this is true for the RDI and temperature variables as well as RDI and SPI. In November, the relationship between RDI and temperature, as well as RDI and precipitation, SPI and precipitation, and RDI and SPI were significant (adjusted R^2 = 0.4759, 0.6838, 0.9459, and 0.7603, respectively), indicating the harmony of changes in the dependent variables in response to changes in the explanatory variable. In other words, the explanatory variable in the above regression model accounts for 47.59%, 68.38%, 94.59%, and 76.03% of the variation in the dependent variable, or serves as a good estimator for the dependent variable. The AIC values, the joint F-statistic, and the joint Wald statistic also confirm the significance of the relationship at the 0.05 level. The Koenker (BP) statistic is a test that assesses the stability of the relationship between the explanatory variables and the dependent variable across both geographic and data space. The null hypothesis of this test asserts the stationarity of the model. Therefore, at the 95% confidence level, a p-value (probability) less than 0.05 indicates heteroscedasticity and/or non-stationarity and statistical significance. Here, the p-value for this test is less than 0.05. Consequently, the assumption of homoscedasticity or stationarity is rejected, and the alternative hypothesis—positing heteroscedasticity or non-stationarity—is accepted. Therefore, the relationship between the explanatory and dependent variables lacks stability, both in geographic and data space. Also, the Jarque-Bera statistic, which is used to test the normality of the residuals, shows that, because the p-value is smaller than 0.05, the residuals do not have a normal distribution in the three months of the autumn season. Given the heterogeneity, it can be expected that there is a cluster pattern in the space under study.

The results obtained from Anselin Local Moran's I statistic indicate that the variables of temperature, precipitation, the RDI index, and the SPI index follow HH and LL clustering patterns. In other words, ALMI shows similar positive values in the form of both HH and LL patterns. The clustering pattern of the temperature variable indicates a lack of correspondence and a disharmony between this variable and the RDI index during the months of October and December. As can be observed, the temperature variable is characterized by an HH pattern in the central part—with a tendency toward its western side—and an LL pattern in the eastern and northwestern portions of this region. The precipitation variable shows good harmony with the RDI index. However, the adjusted R^2 value between precipitation (the explanatory variable) and SPI (the dependent variable) in October is very low (0.0573). Despite the weak relationship between these two variables in October, a spatial harmony between their HH and LL clusters is observed (Table 9 and Fig 7).

Table 9. Ordinary Least Squares (OLS) regression of Moran's I statistics for temperature, precipitation, RDI, and SPI during the autumn months

Variables and Statistics	**Autumn Season**											
	October				**November**				**December**			
Dependent Variable	RDI	RDI	SPI	RDI	RDI	RDI	SPI	RDI	RDI	RDI	SPI	RDI
Explanatory Variable	T	P	P	SPI	T	P	P	SPI	T	P	P	SPI
Intercept	-0.157740	-0.04515	0.028826	-0.059982	0.060705	0.080020	0.001900	0.078028	-0.067065	-0.128180	-0.000054	-0.128204
Coefficient	0.272708	0.75637	-0.359939	-0.155141	0.485323	0.447663	0.946841	0.484853	-0.227322	0.137139	1.000138	0.134220
AICc	-60625	-76612	-46594	-60981	-63607.8	-70816	-79256	-74766	-46429	-45568	-194627	-45561.8
Multiple R^2	0.0418	**0.6875**	0.0573	0.0654	**0.4759**	**0.6838**	**0.9459**	**0.7603**	0.0685	0.0106	**0.9999**	0.010136
Adjusted R^2	0.04169	**0.6875**	0.0572	0.0653	**0.4759**	**0.6838**	**0.9459**	**0.7603**	0.0684	0.01051	**0.9999**	0.010067
Joint F-Statistic	621.7	31387	866.897	998.42	12956.7	30853	249384	45245	1049	152.51	279602043	146.07
Joint Wald Statistic	473.26	47343	684.913	1368.7	10309.34	22071	353426	42034	1638	145.90	252573935	140.67
Koenker (BP) Statistic	289.13	67.3027	206.48	1.404	1362.8	614.44	335.83	457.37	360.04	1116.89	308.33	1086.38
Jarque-Bera Statistic	231.25	146.5987	228.347	282.4179	152.62	10589.7	52785	12270.9	5299.8	1514.48	3767.46	1534.47

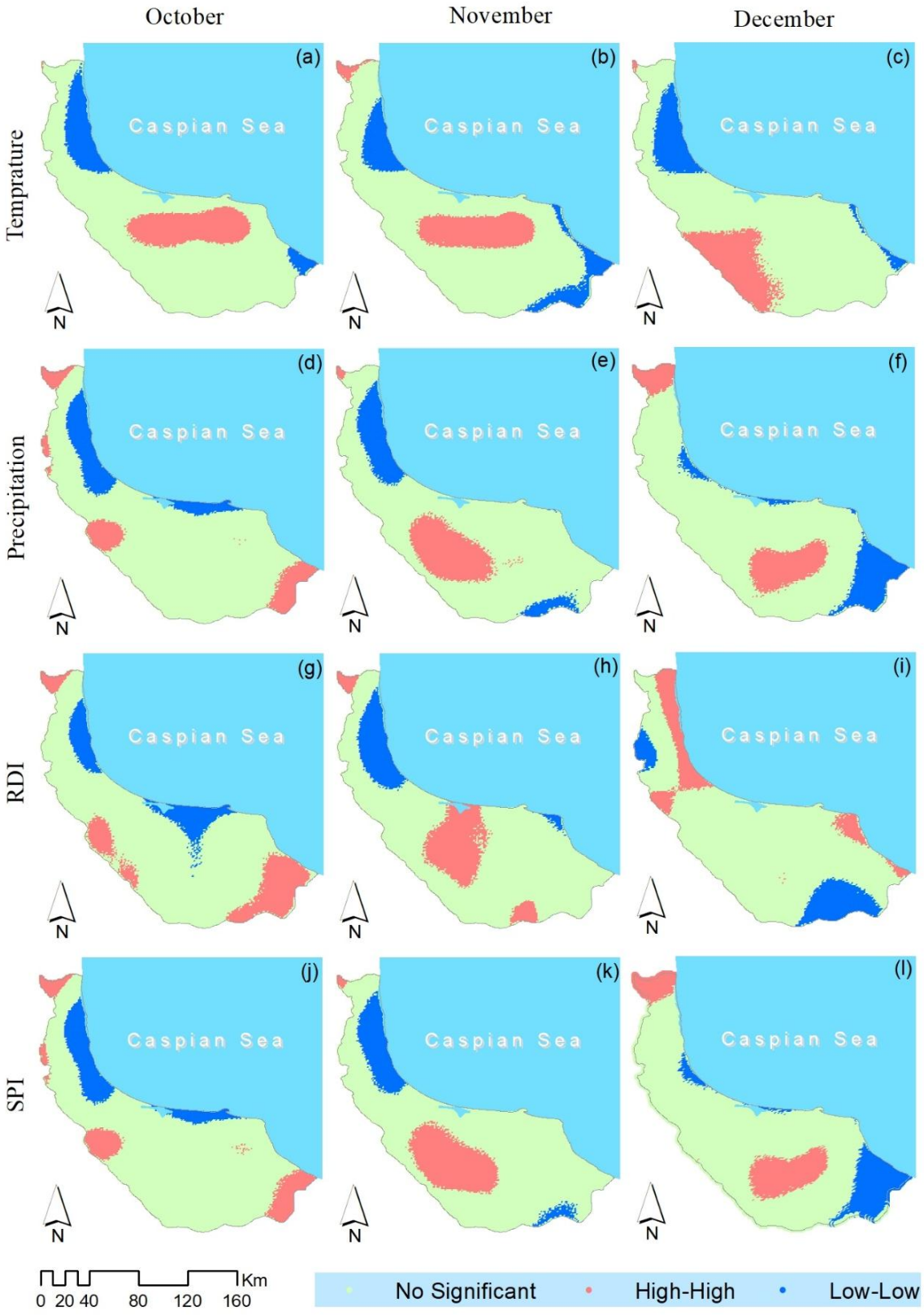


Fig 7. Anselin Local Moran's I (ALMI) statistics for temperature, precipitation, and the RDI and SPI drought indices, used to identify clusters and outliers, as well as their spatial harmony and disharmony during the autumn months.

Despite good harmony between precipitation (the explanatory variable) and the RDI in October, the strength of the relationship has decreased somewhat. This also applies to the month of November. The OLS regression relationship between SPI and precipitation indicates the strength of the association between these two variables, as well as the harmony of the HH and LL spatial patterns in November. In this month, the HH cluster is observed in the central part of Guilan province and the LL cluster is observed in the northwest, and their spatial harmony is high. The patterns that have emerged for the RDI index and for precipitation during the month of November are somewhat similar. Ultimately, the Anselin Local Moran's I statistic indicates that, in addition to a high adjusted R^2 value in December, the spatial patterns of the SPI and precipitation are similar and exhibit consistent behavior.

4. Discussion and Conclusion

A precise analysis of the spatiotemporal trends in temperature, precipitation, and the RDI and SPI indices—as well as the spatial patterns and spatial harmony of variations in these variables across Guilan Province—can assist in identifying spatially homogeneous units and gaining a better understanding of them. To achieve this goal, temperature and precipitation data for Guilan province were analyzed in the form of 0.25° × 0.25° cells from the European Centre for Medium-Range Weather Forecasts (ECMWF) for 44 years. In addition to these two variables, evapotranspiration was calculated using the Thornthwaite method and employed to determine drought severity using the Reconnaissance Drought Index (RDI). In addition to the RDI index, the SPI index was also used. Through the Mann-Kendall trend test, the trend of temperature, precipitation, RDI and SPI indices and their significance were determined. Furthermore, OLS regression was employed to estimate the dependent variables RDI and SPI using temperature and precipitation as explanatory variables. Then, the spatial pattern of the Mann-Kendall statistic of the four variables temperature, precipitation, RDI index, and SPI was determined in the area of Guilan province using the Anselin Local Moran's I Index (ALMI). An analysis of temperature indicates an increasing trend over the 44-year period. An upward trend was confirmed in the average temperature of the province, as well as across all cells. Given the significance of rising temperatures in recent decades, this phenomenon has also been confirmed by other researchers, including Asakereh et al. (2019), who reported that temperatures in Iran have risen significantly over the past few decades. For example, the country's temperature increased by 0.17 and 0.1 °C during the decades 1990–2000 and 2001–2010, respectively, compared to the 1961–1970 decade. Meanwhile, temperatures in Iran showed a decrease of 0.03 °C during the decades 1961–1970 and 1981–1990. Also, a study by Saboohi et al. (2012) on temperature trends in Iran showed that most stations, especially those located in the western and eastern parts of the country, show a significant positive trend in

563 the monthly temperature time series of the summer season. However, the highest number of stations with a positive
564 trend was observed in April (30 stations) and August (29 stations), while the highest number with a negative trend was
565 seen in February (16 stations) and March (15 stations). As a result, there is consistency between the results obtained
566 from the temperature variation trend in Guilan Province and other studies conducted in the country, and all of them
567 emphasize its increasing trend in the last few decades. In addition to the existence of a trend in temperature in Guilan
568 Province, the existence of a trend in precipitation during the warm months of the year (May, June, and August) was
569 also confirmed. The decreasing trend in precipitation in May, June, and August has had a direct impact on the
570 ecological conditions of this area of the country. Also, the decrease in precipitation and its irregularity have led to a
571 decrease in surface and groundwater resources, which has resulted in farmers facing difficulties in obtaining the water
572 needed for agriculture. The issue of decreased precipitation and irregularity in its occurrence has been studied by other
573 researchers. For example, Feizi et al. (2014) showed that precipitation in the southeast of the country had a negative
574 trend during the summer and autumn seasons, with a lower trend in the spring and no trend in the winter. Raziei et al.
575 (2014) examined the spatial pattern and temporal trend of precipitation in Iran and concluded that annual precipitation
576 has a decreasing trend in the northwest and southeast of the country and an increasing trend in the western, central,
577 and northeastern regions. Also, in winter and autumn, an increasing trend is observed in most parts of the country,
578 with the exception of the northwest and southeast, where a decreasing trend prevails. During spring and summer, a
579 decreasing trend in precipitation prevails across most regions of Iran. Overall, Iran's precipitation follows a decreasing
580 trend in spring and summer and an increasing trend in autumn and winter. Given the decreasing trend in precipitation
581 during the warmer months of the year in Guilan Province—and the lack of a statistically significant trend during the
582 colder months—there is a degree of alignment between the findings of this study and the aforementioned research
583 conducted across Iran.
584 In addition, a detailed analysis of the variations in the RDI and SPI indices was performed using the Mann-Kendall
585 trend test, determining the type of trend in the RDI and SPI indices and their significance. Also, the spatial pattern and
586 spatial harmony or disharmony of the Mann-Kendall statistic of these two drought indicators across Guilan province
587 were determined using the OLS regression model and the Anselin Local Moran’s I (ALMI). An examination of the
588 RDI and SPI trends in Guilan province showed that the negative trend in both indices occurred in the warm months
589 of the year and the intensity of this phenomenon has increased in recent decades. In this regard, the results of other
590 studies show that drought severity classes 4 and 3 of the SPI index have the highest frequency of occurrence, while

591 classes 6 and 7 have the lowest frequency of occurrence. Also, the SPI time series of 84.21% of the stations studied
592 across Iran showed a negative trend during the years 1967 to 2014 (Bahrami et al., 2019). Shafizadeh et al. (2016)
593 examined the spatial-temporal variability of drought trends using the RDI index across Iran and concluded that 89%
594 of the studied stations showed a decreasing trend in the RDI index. Also, Asadi Zareh et al. (2011) reported that during
595 1999 and 2000, the central, eastern, and southeastern parts of Iran faced severe drought conditions. According to the
596 trends in the RDI and SPI indices, other parts of the country are experiencing severe droughts. Therefore, the results
597 obtained from the RDI and SPI index trends in this study are consistent with those of other studies in other regions of
598 the country, and the existence of a trend in these two indices is confirmed by the existence of a trend in the precipitation
599 and temperature variables of Guilan province during the warm period of the year.
600 Also, the results obtained from ordinary least squares (OLS) regression between the RDI variable and temperature,
601 RDI and precipitation, SPI and precipitation, and RDI and SPI showed that temperature is not a suitable variable for
602 estimating the RDI and SPI indices, but there is a strong relationship between SPI and precipitation in the winter
603 months.
604 Therefore, there is a good spatial harmony between precipitation and SPI variations in the study area, and considering
605 the instability of variance in this area, the HH and LL patterns of the Local Moran's I statistic are completely consistent.
606 In the spring months, in addition to the strong relationship between SPI and precipitation, the relationship between
607 RDI and precipitation and RDI and SPI is significant at the 0.05 significance level and the intensity of the relationship
608 is high. The intensity of the relationship has led to a good spatial harmony between them. The conditions governing
609 the relationship between the aforementioned variables in the spring have also been repeated in the summer. In other
610 words, the relationship between SPI and precipitation is extremely strong, and the relationship between the other two
611 variables is also highly significant. In autumn, the relationship between SPI and precipitation was not significant only
612 in October, when there was a good relationship only between RDI and precipitation. In November, there is a
613 relationship between all four variables, and in December, only the relationship between SPI and precipitation is
614 significant. Given the good relationship between the variables, the explanatory variable can be used to estimate the
615 dependent variables, including SPI and RDI. As a result, instead of long and laborious SPI calculations, the regression
616 relationship between the two can be used for prediction.
617 Finally, spatial analysis of the RDI and SPI indices showed that a high-high (HH) cluster pattern was formed in months
618 when the trend in the aforementioned variables was significant. High-high (HH) clusters were visible as separate areas

across the province from east to west and from plains to mountains. As a result, the spatial distribution of the RDI and SPI indices based on the Anselin Local Moran's I Index (ALMI) indicates the presence of a cluster structure in the months when there was a trend in the two indices in question. In addition, the non-random structure in the studied patterns indicates a kind of homogeneity and harmony between the values of the variables in the study area.

Author contributions All authors participated in the initial design, data collection, analysis, and writing of the draft of the article, and they all read and approved its text.

Funding This research did not use financial resources from any organization or institution.

Data availability The data required for this study were obtained from the Iranian Meteorological Organization. MODIS Terra satellite images were also obtained from the https://earthexplorer.usgs.gov/ and upper atmosphere data were obtained from the NCAR/NCEP reanalysis data 1.

Declarations

Conflict of interest The authors have no competing interests to declare that are relevant to the content of this article.

Consent to participate All authors consent to participate.

Consent for publication All authors consent to publish this work.

References

Alina, V., Irina, O. (2013). Summer air temperature variability and trends within Oltenia Plain. *Journal of the Geographical Institute "Jovan Cvijic*, 63 (3), 371-381. https://doi.org/10.2298/IJGI1303371V

Asadi Zareh, M. A., Malekinezhad, H., Mobin, M. H., Dastorani, M. T., Kousari, M. R. (2011). Drought Monitoring by Reconnaissance Drought Index (RDI) in Iran. *Water Resour Manage*, 25, 3485–3504. https://doi.org/10.1007/s11269-011-9867-1

Asakereh, H., Khosravi, Y., Doostkamian, M., & Solgimoghaddam, M. (2019): Assessment of Spatial Distribution and Temporal Trends of Temperature in Iran. *Asia-Pacific Journal of Atmospheric Sciences*, 56, 549–561. https://doi.org/10.1007/s13143-019-00150-9

Bahrami, M., Bazrkar, S., Zarei, A. R. (2019). Modeling, prediction and trend assessment of drought in Iran using standardized precipitation index. *Journal of Water and Climate Change*, 10 (1), 181–196. https://doi.org/10.2166/wcc.2018.174

Bazrafshan, O., Mahmudzadeh, F., Bazrafshan, J. (2017). Evaluation of temporal trends of the drought indices SPI and SPEI in the Southern Coast of Iran. *Desert Management*, 4(8), 54-69. https://doi.org/10.22034/jdmal.2017.24662

Chirgwin, R. (2012). Ocean currents emerge as climate change hot-spots. The Register, available at <http://www.theregister.co.uk> (accessed Feb. 2012).

Darand M. (2015). Assessment and Detection of Climate change in Iran during Recent Decades. *Iranian Journal of Watershed Management Science and Engineering*, 9 (30), 1-14. URL: http://jwmsei.ir/article-1-537-fa.html

Derakhshi, J., Sobhani, B., Jahanbakhsh, S. (2024). Forecasting temperature and precipitation values over the coming decades using the CanESM2 model In the Ahrchai watershed. *Journal of Applied Researches in Geographical Sciences*, 24(72), 49-64. http://dx.doi.org/10.52547/jgs.24.72.49

Dottori, F., Szewczyk, W., Ciscar, J.-C., Zhao, F., Alfieri, L., Hirabayashi, Y., et al. (2018): Increased human and economic losses from river flooding with anthropogenic warming. *Nature Climate Change*, 8 (9), 781–786. https://doi.org/10.1038/s41558-018-0257-z

Doulabian, S., Golian, S., Shadmehri Toosi, A., & Murphy, C. (2021). Evaluating the effects of climate change on precipitation and temperature for Iran using RCP scenarios. *Journal of Water and Climate Change*, 12 (1), 166–184. https://doi.org/10.2166/wcc.2020.114

Feizi, V., Mollashahi, M., Farajzadeh, M., Azizi, G. (2014): Spatial and Temporal Trend Analysis of Temperature and Precipitation in Iran. *EcoPersia*, 2 (4) ,727-742. http://ecopersia.modares.ac.ir/article-24-6002-en.html

Gao, Y., Fu, Sh., Cui, H., Cao, Q., Wang, Z., Zhang Z., Wu, Q., Qiao, J. (2023). Identifying the spatio-temporal pattern of drought characteristics and its constraint factors in the Yellow River Basin. *Ecological Indicators*, 154, 110753. https://doi.org/10.1016/j.ecolind.2023.110753

Ghaemi, A., Hashemi Monfared, S. A., Bahrpeyma, A., Mahmoudi, P., Zounemat-Kermani, M. (2022). Spatiotemporal variation of projected drought characteristics of Iran under the climate change scenarios. *Journal of Meteorology and Atmospheric Science*, 5(1), 68-80. https://doi.org/10.22034/jmas.2023.390166.1199

Ghiasabadi Farahani, F., khoshakhlagh, F., Shamsipour, A., Azizi, G., fattahi, E. (2018). Analysis of inter-decade changes in trends and spatial patterns of annual and seasonal precipitation, case study: West of Iran. *Journal of Applied Researches in Geographical Sciences*, 18(48), 59-78. http://dx.doi.org/10.29252/jgs.18.48.59

Gilbert, R. O. (1987). Statistical methods for environmental pollution monitoring. Van Nostrand Reinhold, New York.

Gomez-Gomez, J. D. D., Velazquez, D. P., Collados-Lara, A. J., Chacon, F. F. (2022). The impact of climate change scenarios on droughts and their propagation in an arid Mediterranean basin. A useful approach for planning adaptation strategies. *Science of The Total Environment*, 820, 153128, https://doi.org/10.1016/j.scitotenv.2022.153128

IPCC (Intergovernmental Panel on Climate Change). (2023). Climate Change 2022 Mitigation of Climate Change. *Working Group III Contribution to the Sixth Assessment Report of the Intergovernmental Panel on Climate Change*. DOI: 10.1017/9781009157926

Liu, Ch., Yang, C., Yang, Q., Wang, J. (2021). Spatiotemporal drought analysis by the standardized precipitation index (SPI) and standardized precipitation evapotranspiration index (SPEI) in Sichuan Province, China. *Scientific Reports*, 11, 1280. https://doi.org/10.1038/s41598-020-80527-3

Marques desa, J. P. (2003). Applied statistics using Spss, Statistica and Mat lab. University of parto, pub in Springer – ver lag Berlin Heidelberg, pp395.

Mathbout, S., Martin-Vide, J., & Bustins, J. A. L. (2023). Drought characteristics projections based on CMIP6 climate change scenarios in Syria. *Journal of Hydrology: Regional Studies*, 50, 101581. https://doi.org/10.1016/j.ejrh.2023.101581

Mirabassi, R., and Dinpazhooh, Y. (2013). Trend Analysis of Precipitation of NW of Iran Over the Past Half of the Century. *Irrigation Sciences and Engineering*, 35(4), 59-73. https://jise.scu.ac.ir/article_10799.html?lang=en

Mirshekaran, Y., Kakapour, V., Zarey, A. (2021). Assess the effect of climate change on precipitation and temperature using AR4 models (Case Study: Gharasoo Basin of Kermanshah province). *Climate Change Research*, 2(8), 23-34. https://doi.org/10.30488/ccr.2022.319044.1061

Mohammadi, N., Hedjazizadeh, Z., Zeaiean Firouzabadi, P., Karbalaee Doree, A., Galehban, E., Alavi Panah, K. (2026). Assessment of the impacts of climate change on land surface temperature and drought risk in agricultural land use in Khuzestan province. *Water and Soil Management and Modelling*, 6(1), 164-191. https://doi.org/10.22098/mmws.2025.18202.1658

Nejadrekabi, M., Eslamian, S., Zareian, M. J. (2021). Using spatial statistics to identify drought-prone regions (A case study of Khuzestan Province, Iran). *Advances in Environmental Technology*, 7(4), 231-262. https://doi.org/10.22104/aet.2022.5143.1397

Nicholson, S. E., Funk, C., Fink, A. H. (2018). Rainfall over the African continent from the 19th through the 21st century. Global and Planetary Change, 165, 114-127. https://doi.org/10.1016/j.gloplacha.2017.12.014

Nkeki, F. N., & Osirike, A. B. (2013). GIS-Based Local Spatial Statistical Model of Cholera Occurrence: Using Geographically Weighted Regression. *Journal of Geographic Information System*, 5, 531-542. http://dx.doi.org/10.4236/jgis.2013.56050

Ogunrinde, A. T., Oguntunde, P. G., Akinwumiju, A. S., Fasinmirin, J. T., Olasehinde, D. A., Pham, Q. B., Linh, N. T. T., & Anh, D. T. (2022). Impact of Climate Change and Drought Attributes in Nigeria. *Atmosphere*, 13(11), 1874. https://doi.org/10.3390/atmos13111874

Pirnia, A., Habibnejad Roshan, M., Soleimani, K. (2015). Investigation of Precipitation and Temperature Changes in Caspian Sea Southern Coasts and Its Comparison with Changes in Northern Hemisphere and Global Scales. *Journal of Watershed Management Research*, 6(11), 90-100. URL: http://jwmr.sanru.ac.ir/article-1-495-en.html

Raftery, A. E., Zimmer, A., Frierson, D. M. W., Startz, R., & Liu, P. (2017): Less than 2°C warming by 2100 unlikely. *Nature Climate Change*, 7 (9), 637–641. https://doi.org/10.1038/nclimate3352

Raziei, T., Daryabari, J., & Bordi, I., & Pereira, L. S. (2014): Spatial patterns and temporal trends of precipitation in Iran. *Theor Appl Climatol*, 115: 531–540. https://doi.org/10.1007/s00704-013-0919-8

Roshani, M., Ramazanipour, M., Tatina, M., Robati, M. (2012). Characteristics of Drought in Three Recent Decades in North of Iran, Guilan Province. *American-Eurasian J. Agric. & Environ. Sci*, 12 (1), 115-122.

Roshani, M., Rezaei, P., Ganji Guofali, S. (2021). Statistical Analysis of Geographic information with ArcView and ArcGIS. Divid S W Wang & Jee Lee, Jahad Daneshgahi Environment Research Press, First publication, 388 Page.

Saboohi, R., Soltani S., Khodagholi, M. (2012): Trend analysis of temperature parameters in Iran. *Theor Appl Climatol*, 109, 529–547. https://doi.org/10.1007/s00704-012-0590-5

Sayat, A., Lyazzat, M., Elmira, T., Gaukhar, B., Gulsara, M. (2025). Assessment of the impacts of climate change on drought intensity and frequency using SPI and SPEI in the Southern Pre-Balkash region, Kazakhstan. *Watershed Ecology and the Environment*. 7, 11–22. https://doi.org/10.1016/j.wsee.2024.12.001

Shafizadeh, F., Naser-Sadrabadi, A., Rostami, N. (2016). Assessing spatiotemporal variability of drought trend in Iran using RDI index. *Natural Environment Change*, 2 (1), 67- 77.

Shi, Ke., Touge, Y., Kazama, S. (2022). Defining Homogeneous Drought Zones Based on Soil Moisture across Japan and Teleconnections with Large-Scale Climate Signals. *Journal of Applied Meteorology and Climatology*, 61(1), 43-60. https://doi.org/10.1175/JAMC-D-21-0133.1

Shi, X., Han, W., Wang, Y. (2025). Spatial heterogeneity of agricultural drought drivers in irrigation district: A causal inference framework bridging covariation and structural equation modeling. *Agricultural Water Management*, 322, 109978. https://doi.org/10.1016/j.agwat.2025.109978

Soleimani Sardoo, F., Mesbahzadeh, T. (2021). The Prediction of Temperature and Precipitation Using Climate Change Scenarios and Statistical Exponential Downscaling Models. *Environmental Researches*, 11(22), 97-110. https://www.magiran.com/p2305125

Sun, Q., Miao, C., Hanel, M., Borthwick, A. G. L., Duan, Q., Ji, D., & Li, H. (2019): Global heat stress on health, wildfires, and agricultural crops under different levels of climate warming. *Environment International*, 128, 125–136. https://doi.org/10.1016/j.envint.2019.04.025

Surampalli, R. Y., Zhang, T. C., Ojha, C. S. P., Gurjar, B., Tyagi, R. D., Kao, C. M. (2013). Impact of Greenhouse Gas Emissions and Climate Change. Authors: Zhang, T. C., and Surampalli, R. Y., Chapter 5, PP92-108.

Surendran Nair, S., King, A. W., Gulledge, J., Preston, B. L., McManamay, R. A., & Clark, C. D. (2020): Economic losses from extreme weather in the U.S. Gulf Coast region: Spatially differential contributions of climate hazard and socioeconomic exposure and vulnerability. *Environmental Research Letters*, 15 (7), 074038. https://doi.org/10.1088/1748-9326/ab7b9a

Tsakiris, G., & Vangelis, H. (2004). Towards a Drought Watch System Based on Spatial SPI. *Journal of Water Resources Management*, 18, 1–12. https://doi.org/10.1023/B:WARM.0000015410.47014.a4

Wang, S., Xu, K., Ma, X., Hu, W., Zhao J., Wang, F., Su, D., Zhang, Z., Wu, Y., Li, M. (2025). Characteristics of spatial and temporal changes of drought in the Inner Mongolia section of the Yellow River Basin based on geodetector. *Frontiers in Climate*, 7:1656424. https://doi.org/10.3389/fclim.2025.1656424

Watts, N., Amann, M., Arnell, N., Ayeb-Karlsson, S., Beagley, J., Belesova, K., et al. (2020). The 2020 report of the Lancet Countdown on health and climate change: Responding to converging crises. *The Lancet*. https://doi.org/10.1016/s0140-6736(20)32290-x

Zahid, M., Rasul, G. (2010). Rise in Summer Heat Index over Pakistan. *Journal of Meteorology*, 6. https://api.semanticscholar.org/CorpusID:133937619

Zarrin, A., Dadashi-Roudbari, A. (2022). Technical Note: Assessing the Effect of Climate Change on Heavy Precipitation in Iran Based on a CMIP6 Ensemble Model. *Journal of Water and Sustainable Development*, 8(4), 119-124. https://dor.isc.ac/dor/20.1001.1.24235474.1400.8.4.14.9

Zarrin, A., Dadashi-Roudbari, A. (2023). Investigating the Impacts of Climate Change on Water Security in Iran. *Journal of Water and Sustainable Development*, 10(1), 37-44. https://doi.org/10.22067/jwsd.v10i1.2301-1210